Epigenetics Insights

ARTICLE

Open Access

https://doi.org/10.48130/epi-0025-0016

Epigenetics Insights **2026**, 19: e002

m^{6}A-mediated epitranscriptomic remodeling coordinates lipid metabolism and transcriptional networks during porcine adipocyte differentiation

Liqiang Xie[1,2#], Juan Huang[1#*], Tianxia Liu[3,4#], Yang Liu[5,6#], Quan Wang[5], Ming Wang[1], Jinfeng Chen[1], Xiaoming Zhang[1,2*] and Jianguo Zhao[3,4*]

[1] *State Key Laboratory of Animal Biodiversity Conservation and Integrated Pest Management, Institute of Zoology, Chinese Academy of Sciences, Beijing 100101, China*
[2] *College of Life Sciences, University of Chinese Academy of Sciences, Beijing 100049, China*
[3] *State Key Laboratory of Organ Regeneration and Reconstruction, Institute of Zoology, Chinese Academy of Sciences, Beijing 100101, China*
[4] *Beijing Institute for Stem Cell and Regenerative Medicine, Beijing 100101, China*
[5] *Shenzhen Branch, Guangdong Laboratory of Lingnan Modern Agriculture, Genome Analysis Laboratory of the Ministry of Agriculture and Rural Affairs, Agricultural Genomics Institute at Shenzhen, Chinese Academy of Agricultural Sciences, Shenzhen 518120, China*
[6] *Department of Clinical Research and Translational Medicine, The Third Affiliated Hospital of Zhengzhou University, Zhengzhou 450052, China*
[#] Authors contributed equally: Liqiang Xie, Juan Huang, Tianxia Liu, Yang Liu
[*] Correspondence: huangjuan@ioz.ac.cn (Huang J); zhangxm@ioz.ac.cn (Zhang X); zhaojg@ioz.ac.cn (Zhao J)

Abstract

N^6-methyladenosine (m^{6}A) is the predominant internal modification occurring within RNA molecules, but its role in porcine adipogenesis remains poorly understood. A high-quality transcriptome-wide m^{6}A methylation map was therefore generated, and the m^{6}A regulator expression pattern profiled during the differentiation of stromal vascular fraction cells into white adipocytes. It was found that the demethylases *FTO* and *ALKBH5* were highly expressed in mature adipocytes, accompanied by widespread m^{6}A hypo-methylation. The hypo-methylated gene set was enriched with regulators of metabolism and transcription, and their downregulation suggests that demethylation contributes to transcriptional repression during terminal differentiation. Notably, many hypo-methylated and downregulated genes overlapped with cancer-related pathways, including therapeutic targets such as *ABL1*, *BRCA2*, *MET*, and *PML*. MeRIP-qPCR and RT-qPCR validation confirmed these trends. Together, the present findings demonstrate that m^{6}A demethylation reshapes gene expression to regulate porcine adipocyte differentiation and provides insights into the potential crosstalk between lipid metabolism and oncogenic signaling.

Citation: Xie L, Huang J, Liu T, Liu Y, Wang Q, et al. 2026. m^{6}A-mediated epitranscriptomic remodeling coordinates lipid metabolism and transcriptional networks during porcine adipocyte differentiation. *Epigenetics Insights* 19: e002 https://doi.org/10.48130/epi-0025-0016

Introduction

Pigs (*Sus scrofa domesticus*) are a major source of high-quality, nutritious meat worldwide. However, excessive fat deposition adversely affects pork quality, production efficiency, and growth performance[1,2]. Beyond agriculture, pigs are also an invaluable animal model for studying human diseases[3,4]. With the increasing prevalence of obesity and fatty liver disease globally[5,6], elucidating the mechanisms underlying porcine fat deposition has both agricultural and biomedical significance.

N^6-methyladenosine (m^{6}A) is the most abundant internal modification in eukaryotic mRNAs and long non-coding RNAs, playing a dynamic role in post-transcriptional regulation[7,8]. This reversible modification occurs at the nitrogen-6 position of adenosine, predominantly within the consensus RRACH motif (where R represents A or G, and H represents A, C, or U), with a preference for the GAC context[9,10]. Methyltransferase 'writers', such as METTL3 and METTL14 catalyzed m^{6}A site deposition[11,12], m^{6}A is removed by demethylase 'erasers' such as FTO and ALKBH5[13,14], and interpreted by m^{6}A 'readers' including YTHDF1/2/3, YTHDC1/2, and IGF2BP1/2/3[15–20]. Together, these regulators orchestrate the functional landscape of the epitranscriptome.

The m^{6}A modification plays an important role in regulating multiple pivotal processes of RNA metabolism, including mRNA translation efficiency[15], mRNA stability[16], alternative splicing[21], nuclear export[22], and secondary structure remodeling[23,24]. In adipogenesis, m^{6}A modification modulates the stability of genes associated with autophagy and glycolysis, thereby influencing adipocyte development[25,26]. Among m^{6}A-related enzymes, FTO plays a critical role by promoting early adipocyte differentiation through demethylation of *JAK2* mRNA, which stabilizes the transcript and activates the JAK2–STAT3–C/EBPβ pathway[27]. Conversely, FTO suppresses thermogenesis and the white-to-beige transition by reducing the m^{6}A level of *Hif1a* mRNA, and inhibiting its translation[28]. In pigs, METTL3 was shown to inhibit adipogenic differentiation by methylating *PHKG1* and enhancing its stability[29]. Although several m^{6}A-modified targets have been identified in adipocyte differentiation, the transcriptome-wide role of m^{6}A regulators in porcine adipogenesis remains incompletely understood.

Here, transcriptome-wide m^{6}A methylation dynamics were systematically profiled during porcine adipocyte differentiation. The present results uncovered that genes involved in adipogenic differentiation and lipid metabolism undergo coordinated changes in both expression and m^{6}A modification. A strong positive correlation was observed in hypo-methylated and downregulated genes, highlighting a central role for m^{6}A erasers in regulating gene expression in white adipose tissue (WAT). Moreover, enrichment of cancer-related pathways among these genes suggests potential crosstalk between lipid metabolism and oncogenic signaling. Collectively, these findings demonstrate the pivotal function of m^{6}A erasers in

porcine adipocyte differentiation, and identify potential m^{6}A-regulated targets relevant to both metabolic regulation and disease.

Materials and methods

Cell culture and adipocyte differentiation

For cell culture, adipose tissue samples were obtained from 2-week-old piglets, minced, and subsequently digested for 60 min at 37 °C. The digestion was carried out using 2 mg/mL collagenase type I (Sigma) in DMEM/F12 medium supplemented with 1% fatty acid-free bovine serum albumin (BSA, Sigma). Stromal vascular fraction (SVF) cells were filtered through a 70-μm cell strainer and cultured in DMEM/F12 (Gibco) medium containing 10% fetal bovine serum (FBS, Sigma), and 1% penicillin–streptomycin[30].

For white adipocyte differentiation, SVF cells were first grown to confluence. Following confluence, the cells were induced for 5 d with human WAT induction medium. This medium consisted of DMEM/H supplemented with 0.1 μM dexamethasone, 66 nM insulin (Sigma), 0.25 mM isobutylmethylxanthine, 17 μM pantothenate, 20 mM HEPES (pH 7.4), 0.5% FBS, and 33 μM biotin. On day 5, half of the induction medium was replaced with human WAT maturation medium. This medium consisted of DMEM/H supplemented with 0.1 μM dexamethasone, 66 nM insulin (Sigma), 0.25 mM isobutylmethylxanthine, 17 μM pantothenate, 20 mM HEPES (pH 7.4), 10% FBS, and 33 μM biotin. After one day, cells were transferred to complete maturation medium and cultured for an additional 2 d. Fully differentiated adipocytes (day 8) were collected for subsequent experiments.

Total RNA extraction, reverse transcription, and qPCR

Total RNA was extracted using TRIzol reagent (Invitrogen) according to the manufacturer's protocol[30]. First-strand cDNA synthesis was performed with the First-Strand cDNA Synthesis Mix with DNase (Genesand, SR511). Quantitative PCR was performed using SYBR Green Fast Mix (Genesand, SQ410). Relative expression levels were normalized to *18S rRNA* as the internal reference. The sequences for RT-qPCR primers can be found in Supplementary Table S1.

m^{6}A RNA immunoprecipitation sequencing (MeRIP-seq), and MeRIP-qPCR

MeRIP-seq and MeRIP-qPCR were performed as previously described[16] with some modifications. Briefly, total RNA was isolated with TRIzol reagent (Invitrogen) following the manufacturer's instructions. Poly(A)+ RNA was purified using the Dynabeads™ mRNA Purification Kit (Thermo Fisher, 61006), and fragmented into ~200 nt fragments with the RNA Fragmentation Reagent (Thermo Fisher, AM8740). Approximately 100 ng of fragmented RNA was reserved as an input control. For immunoprecipitation, 1 μg of fragmented poly(A)+ RNA was incubated with 2 μg of anti-m^{6}A antibody (Synaptic Systems, 202003) at 4 °C for 3 h, followed by capture with Dynabeads™ Protein A (Thermo Fisher, 10002D) for 2 h at 4 °C. Beads were washed three times with IPP buffer (150 mM NaCl, 0.1% NP-40, 10 mM Tris-HCl, pH 7.4). m^{6}A-enriched RNA was competitively eluted using free m^{6}A nucleotides, precipitated with ethanol, and further purified with the RNeasy MinElute Cleanup Kit (Qiagen, 74204). Libraries were prepared using the KAPA Stranded RNA-Seq Kit (KAPA Biosystems, KK8401) and sequenced on an Illumina NovaSeq 6000 platform (ANOROAD, Beijing, China).

To assess the methylation level of specific transcripts in SVF and WAT cells, MeRIP-qPCR was performed. The m^{6}A-IP procedure was identical to that used for MeRIP-seq. Enriched RNA was eluted with DEPC-treated water, reverse-transcribed using the First-Strand cDNA Synthesis Mix with DNase (Genesand, SR511), and quantified by qPCR. The fraction recovered was calculated relative to the input. A complete list of the MeRIP-qPCR primers used is provided in Supplementary Table S1.

Bioinformatic analysis of MeRIP-seq and RNA-seq data

The raw input RNA-seq and MeRIP-seq data were processed using fastp software (v0.22.0)[31] to remove adaptor contamination and low-quality bases. Fastp outputs were summarized using MultiQC (v1.13.dev0)[32]. Clean reads were mapped to the reference genome of the *Sus scrofa* (version Sscrofa11.1)[33] using HISAT2 (v2.2.1)[34], with the parameters '-k 5 --max-intronlen 317,503 --summary-file'. The unique mapping clean reads were quantified using featureCounts from the subread software (v2.0.1)[35], following analysis of differentially expressed genes was conducted using the R package DESeq2 (v1.38.3)[36]. Genes were considered differentially expressed if they had an absolute $\log_2$foldchange value > 1, and a false discovery rate (FDR) value < 0.05 in the input RNA-seq data. For Principal component analysis, gene expression patterns were calculated on the regularized normalized counts obtained from DESeq2, and visualization using plotPCA. Sample correlation analysis was performed using deeptools software (v3.5.1)[37], Gene Ontology (GO) and Kyoto Encyclopedia of Genes and Genomes (KEGG) functional enrichment analyses were carried out using Bioconductor clusterProfiler (v4.6.2) package[38]. Significantly enriched GO terms (FDR < 0.05) were selected, and visualization analysis using the R package ggplot2 (v3.5.1). Heatmap visualization was performed using the pheatmap (v1.0.12) package in R (v4.2.3) to represent the differentially expressed genes.

For m^{6}A peak calling, the MASC2 peak calling algorithm (https://github.com/macs3-project/MACS/wiki/Install-macs2) were used to identified m^{6}A peaks with the input RNA-seq data as background, and the parameter *q* value was set to 0.05. For each biological replicate, m^{6}A peaks that overlapped at least two of three biological replicates were merged as high confidence m^{6}A peaks using the *slice* function (parameter set to lower = 2, ranges Only = TRUE) in the R package IRanges (https://bioconductor.org/packages/IRanges). The *GuitarPlot* function was used to analyze each conditional high confidence m^{6}A peaks distribution in the R package Guitar (https://github.com/lzcyzm/Guitar). m^{6}A peaks annotation analysis was performed using R package ChIPseeker (v1.34.1)[39]. QNB software (v1.1.11)[40] was used to identify the differential methylational sites. m^{6}A peaks were considered differential methylated peaks if they had an absolute $\log_2$foldchange value > 0.58, and an adjusted *p*-value < 0.05.

Identification of enriched motifs within m^{6}A peaks

To identify significant enriched motifs, *de novo* analysis was conducted on the high-confidence m^{6}A peaks using HOMER software (v4.11)[41], in brief, the sequences of high confidence m^{6}A peaks were extracted as target sequences using the *fastaFromBed* function in BEDTools software (v2.26.0)[42], with background sequences generated using the *shuffle* function. *De novo* motif analysis was subsequently executed through HOMER's findMotifs.pl script.

Gene set enrichment analysis

GSEA was performed to identify biologically relevant pathways exhibiting coordinated expression changes in input RNA-seq data. In brief, KEGG pathway enrichment was analyzed using GSEA implemented with the *gseKEGG* function in clusterProfiler. Genes were ranked by $\log_2$foldchange values from differential expression analysis. The analysis utilized the KEGG database (v2.4.5)[43] with organism code 'ssc'. Significant pathways were identified at the absolute normalized enrichment score (NES) > 1.5, and FDR value < 0.05. Results were visualized using the *gseaplot2* function in the R package enrichplot (https://github.com/YuLab-SMU/enrichplot) with GSEA enrichment score profiles.

Results

Dynamic changes in m^{6}A regulatory factors during porcine adipocyte differentiation

To investigate the role of m^{6}A modification during the *Sus scrofa* adipocyte differentiation, the mRNA expression patterns of m^{6}A regulator genes were examined, including m^{6}A writers, erasers, and readers during the transition from SVF cells to WAT. Distinct temporal expression profiles were observed (Fig. 1).

Most m^{6}A writers' expression level gradually increased during the first 6 d of differentiation but declined sharply in mature WAT (day 8), except for *WTAP*, which peaked on day 2 (Fig. 1a). In contrast, the m^{6}A erasers *ALKBH5* and *FTO* maintained high expression levels in mature adipocytes (day 8) (Fig. 1b). Notably, *FTO* expression remained elevated from day 2 onward, corresponding with its pivotal role in adipogenesis and adipogenic differentiation[44]. These findings imply that m^{6}A writers may function primarily during the early phase of adipogenesis, whereas m^{6}A erasers were active throughout the entire differentiation process.

Corresponding to the elevated expression of m^{6}A writers on day 2, m^{6}A readers also showed high expression on day 2 but displayed divergent trajectories in subsequent stages (Fig. 1c). Among them, *YTHDC1* and *YTHDC2* exhibited a wave-like expression pattern throughout adipogenesis. On the other hand, *YTHDF1* expression level significantly decreased after day 2, whereas *YTHDC2* and *YTHDF3* maintained high expression levels from day 2 to day 8. Together, these regulators cooperate to modulate m^{6}A methylation of target genes during adipogenesis.

WAT enhances lipid metabolism while suppressing stress responses

Transcriptional changes were next characterized by RNA sequencing of SVF cells (pre-differentiation) and WAT cells (post-differentiation), each with three biological replicates (Supplementary Table S2). Pearson correlation analysis, sample-to-sample distance metrics, and principal component analysis (PCA) confirmed high reproducibility (Supplementary Fig. S1).

Differential expression analysis (absolute fold change > 2, FDR < 0.05) identified 3,739 upregulated and 3,560 downregulated genes (Fig. 2a). Among these, lncRNAs accounted for 18.69% of upregulated, and 6.97% of downregulated transcripts (Fig. 2b), suggesting regulatory roles in adipogenesis.

GO and KEGG enrichment revealed that upregulated genes were strongly enriched in lipid metabolism, lipogenesis, and fatty acid synthesis, supporting their roles in adipogenesis and lipid accumulation. Conversely, downregulated genes were enriched in stimulus

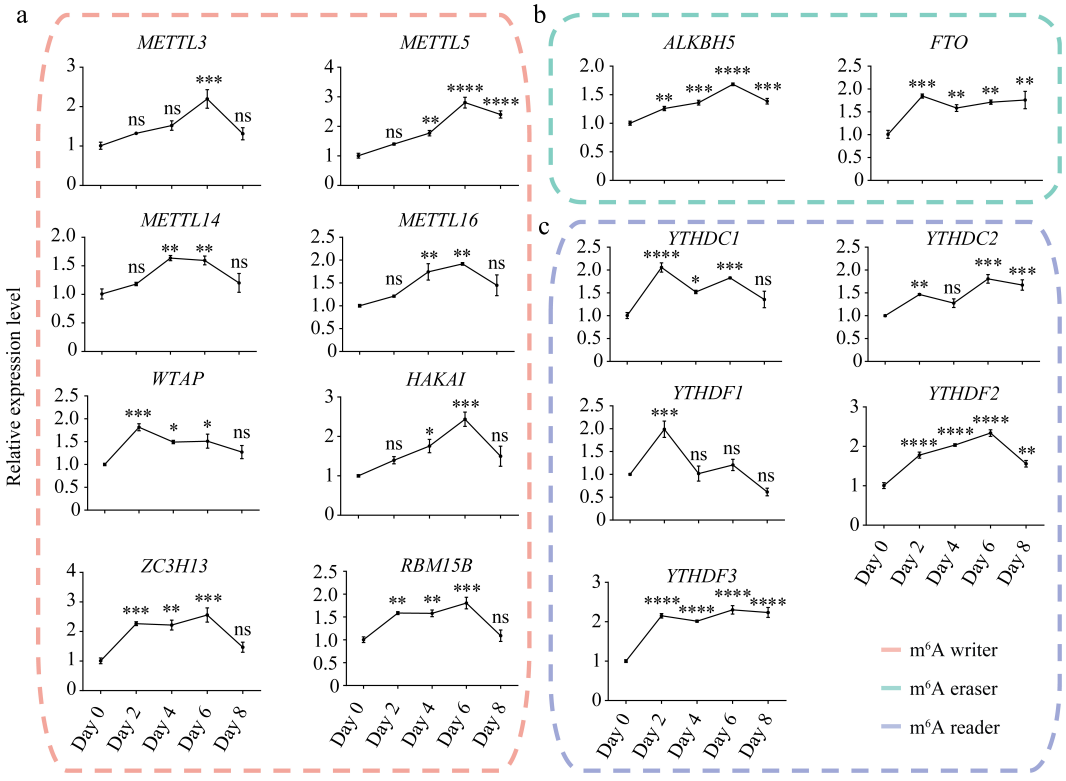

Fig. 1 Expression dynamics of m^{6}A writers, erasers, and readers during porcine adipocyte differentiation. Relative mRNA expression levels of m^{6}A (a) writers, (b) erasers, and (c) readers during SVF adipogenesis. 18S rRNA was used as the internal reference gene. Data are presented as mean ± s.d (n = 3). Statistical significance was determined by ANOVA with a post-hoc test. * $p < 0.05$; ** $p < 0.01$; *** $p < 0.001$; **** $p < 0.0001$; ns, not significant ($p \geq 0.05$).

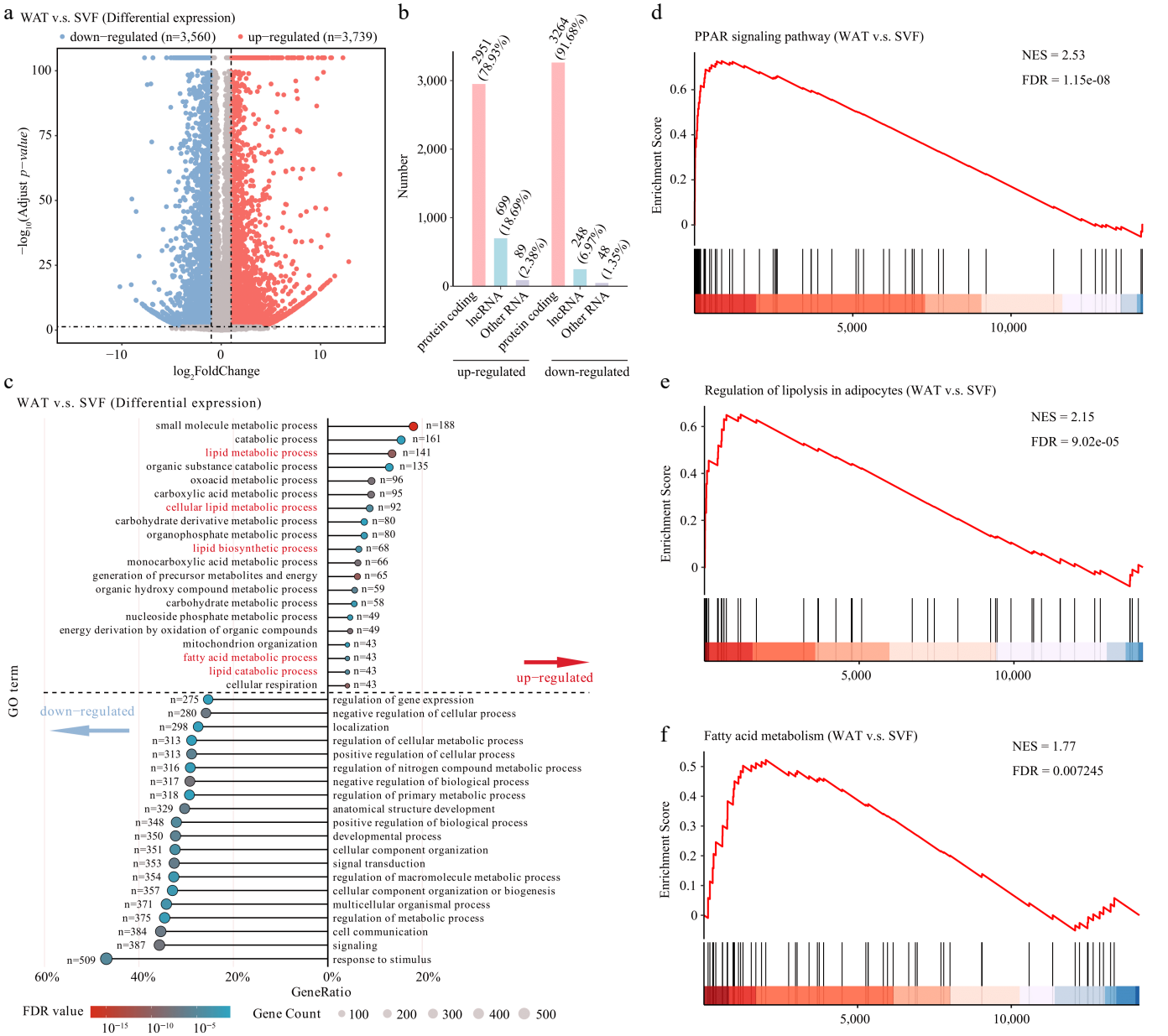

Fig. 2 Transcriptomic reprogramming during porcine adipocyte differentiation. (a) Volcano plot of differentially expressed genes (thresholds: |fold change| > 2, FDR < 0.05). (b) Classification of differentially expressed genes into protein-coding genes, lncRNAs, and other RNA types (including snRNA, snoRNA, miRNA, etc.). (c) GO enrichment analysis of biological processes. Enriched pathways above the dashed line correspond to up-regulated genes, while those below represent down-regulated genes. Terms were considered significantly enriched with an FDR < 0.05. Gene Set Enrichment Analysis (GSEA) of key metabolic pathways. Pathways showing significant enrichment include the (d) PPAR signaling pathway, (e) regulation of lipolysis in adipocytes, and (f) fatty acid metabolism. Normalized enrichment scores (NES) and FDR are indicated for each pathway.

response and regulatory pathways, indicating reduced stress-related activity in mature adipocytes (Fig. 2c).

KEGG further highlighted enrichment of PPAR signaling among upregulated genes (Supplementary Fig. S2)[45], along with fatty acid metabolism and regulation of lipolysis. In contrast, downregulated genes were enriched in PI3K-Akt and MAPK signaling (Supplementary Fig. S2). GSEA confirmed consistent upregulation of PPAR signaling, fatty acid metabolism, and lipolysis-related gene sets in WAT (Fig. 2d–f). Together, these data show that WAT is characterized by enhanced lipid metabolism and reduced stress and signaling activity during differentiation.

Transcriptome-wide mapping reveals positional and functional features of m^{6}A

To profile global m^{6}A changes, MeRIP-seq was performed. Using MACS2 peak calling and requiring overlap in at least two replicates, 18,743 peaks in SVF and 17,790 peaks in WAT were identified (Supplementary Fig. S3a, S3b). m^{6}A peaks were unevenly distributed across chromosomes (Fig. 3a).

At the transcript level, m^{6}A peaks were predominantly enriched in 3'UTRs and CDS regions in both stages, consistent with previous reports (Fig. 3b, c)[46,47]. HOMER motif analysis identified enrichment of GGACH (H = A/C/U) and DGAC (D = A/G/U) motifs, confirming successful enrichment of m^{6}A-modified sequences (Fig. 3d)[29,46,48].

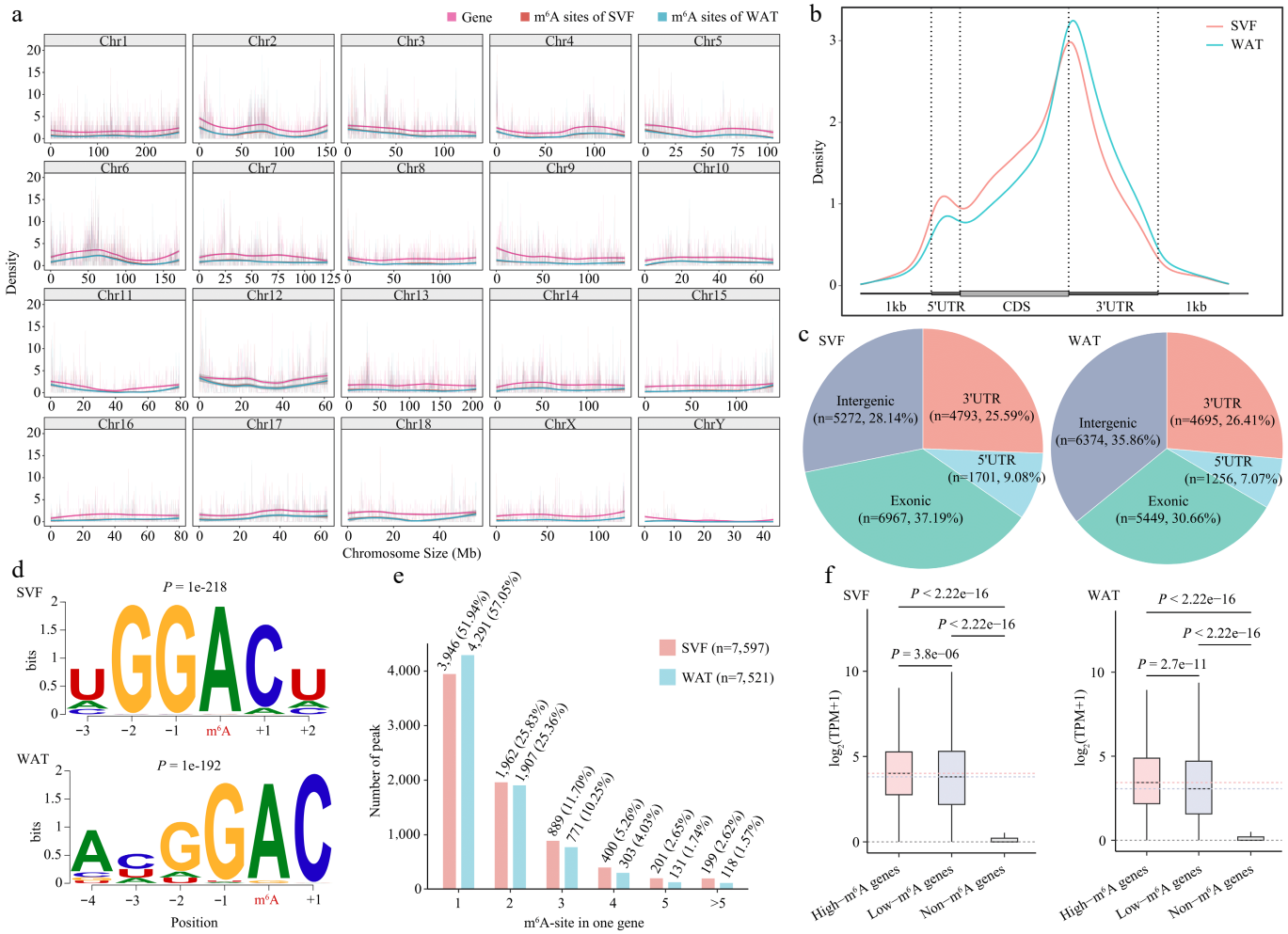

Fig. 3 Transcriptome-wide distribution and features of m^{6}A in porcine adipocytes. (a) Distribution of m^{6}A peaks and gene density across 20 chromosomes in SVF and WAT. (b) Metagene profile of m^{6}A peak distribution across normalized mRNA transcripts, divided into three regions: 5′UTR, coding sequence (CDS), and 3′UTR. Exons are shown as thick boxes and introns as thin lines. (c) Genomic annotation of m^{6}A peaks in SVF and WAT. (d) Consensus sequence motifs of m^{6}A peaks identified by HOMER; red letters indicate the methylated adenine. (e) Abundance of m^{6}A peaks per transcript. The bar chart shows the proportion of transcripts containing different numbers of m^{6}A peaks. (f) Boxplot comparison of expression levels of m^{6}A-modified versus non-m^{6}A-modified transcripts in SVF and WAT. Statistical significance was determined using Student's *t*-test.

Mapping peaks to transcripts revealed 7,597 and 7,521 m^{6}A-modified genes in SVF and WAT, respectively, with more than half containing a single m^{6}A site (Fig. 3e). Approximately 200 lncRNAs carried m^{6}A peaks (Supplementary Fig. S3c). Importantly, transcripts with m^{6}A sites showed significantly higher expression levels than non-m^{6}A-modified transcripts, and those with multiple sites were expressed at higher levels than those with a single site (Fig. 3f), consistent with the role of multiple m^{6}A modifications in stabilizing mRNAs via IGF2BP proteins[20]. Collectively, these results highlight positional enrichment of m^{6}A in CDS and 3′UTRs and its positive association with transcript expression.

m^{6}A demethylation predominates in WAT and targets functional pathways

To assess changes in m^{6}A methylation during porcine adipocyte differentiation, differentially methylated peaks (DMPs) between SVF and WAT (absolute fold change > 1.5, $p < 0.05$) were analyzed. This analysis identified 515 hyper-methylated peaks and 2,112 hypo-methylated peaks (Fig. 4a), corresponding to 230 and 1,304 genes, respectively (Fig. 4b). The predominance of hypo-methylated genes in WAT is consistent with the elevated expression of the m^{6}A erasers *FTO* and *ALKBH5* (Fig. 1). More than 88% of the differentially methylated genes were protein-coding, with a minority being lncRNAs (Fig. 4b). Peak annotation further revealed that hyper-methylated sites were mainly enriched in 5′UTRs, whereas hypo-methylated sites were concentrated in CDS and 3′UTR regions (Fig. 4c).

KEGG functional enrichment analysis revealed differentially methylated genes were enriched in pathways including cancer, MAPK signaling, endocytosis, cAMP signaling, Hippo signaling, oxytocin signaling, and apelin signaling (Fig. 4d, e; Supplementary Fig. S4). Notably, MAPK signaling—critical in adipogenesis and lipid metabolism[49,50]—was among the most enriched categories. These results demonstrate that m^{6}A demethylation predominates in WAT and involves pathways central to adipocyte differentiation.

m^{6}A demethylation represses regulators of metabolism and transcription, including lipogenic genes

To further explore the functional impact of m^{6}A during porcine adipocyte differentiation, transcript abundance and m^{6}A

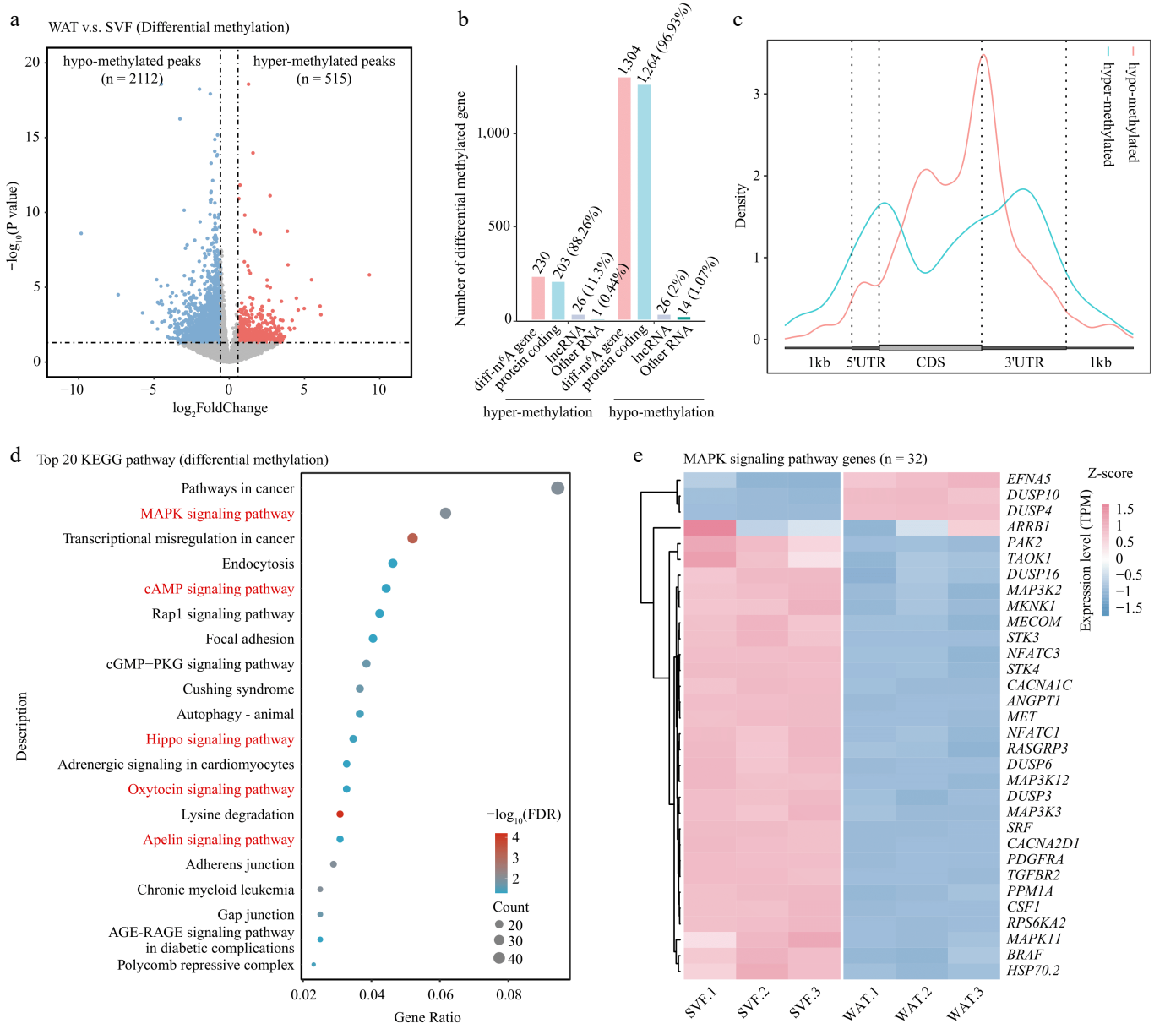

Fig. 4 Differential m^{6}A methylation during porcine adipocyte differentiation. (a) Volcano plot showing differentially methylated m^{6}A peaks between SVF and WAT. Hypermethylated peaks (red) and hypomethylated peaks (blue) represent significant changes, while non-significant peaks are shown in gray. Dashed lines indicate thresholds for fold change and *p*-value. (b) Bar plot showing the numbers and types of genes annotated from differentially methylated peaks. (c) Metagene profile of differential m^{6}A peak distribution across normalized mRNA transcripts. (d) KEGG pathway enrichment analysis of differentially methylated genes presented as a bubble plot. (e) Heatmap of expression levels of MAPK signaling pathway genes in SVF and WAT.

methylation levels were cross-analyzed. Integration of methylation and expression data identified 71 hyper-up, 517 hypo-down, 43 hyper-down, and 122 hypo-up genes (Fig. 5a, Supplementary Table S3). Among 1,304 hypo-methylated genes, 39.6% were downregulated, and only 9.35% were upregulated, suggesting that demethylation destabilizes transcripts in WAT.

Correlation analysis revealed a significant positive association between expression and methylation changes, specifically in hypo-down genes (n = 517). In contrast, no significant correlation was observed in the hypo-up (n = 122), hyper-up (n = 71), and hyper-down (n = 43) categories (Fig. 5b, Supplementary Fig. S5a–S5c). The association between reduced expression and demethylation in hypo-down genes, together with elevated *FTO* and *ALKBH5* expression, underscores the role of m^{6}A erasers in repressing gene expression during terminal adipocyte differentiation. GO enrichment of hypo-down genes revealed enrichment in regulators of metabolic processes and DNA transcription (Supplementary Fig. S5d).

KEGG pathway analysis further showed that many hypo-down genes were enriched in cancer-related pathways. Within this cluster, genes such as *ABL* proto-oncogene 1 (*ABL1*), mesenchymal to epithelial transition factor (*MET*), promyelocytic leukemia nuclear body scaffold (*PML*), and breast cancer susceptibility gene 2 (*BRCA2*)—established oncogenes or therapeutic targets—were downregulated and hypo-methylated in WAT (Fig. 5c, d, Supplementary Table S3). MeRIP-qPCR and RT-qPCR validation confirmed consistent trends between expression and m^{6}A modification levels, supporting the reliability of our sequencing data (Fig. 5e, f).

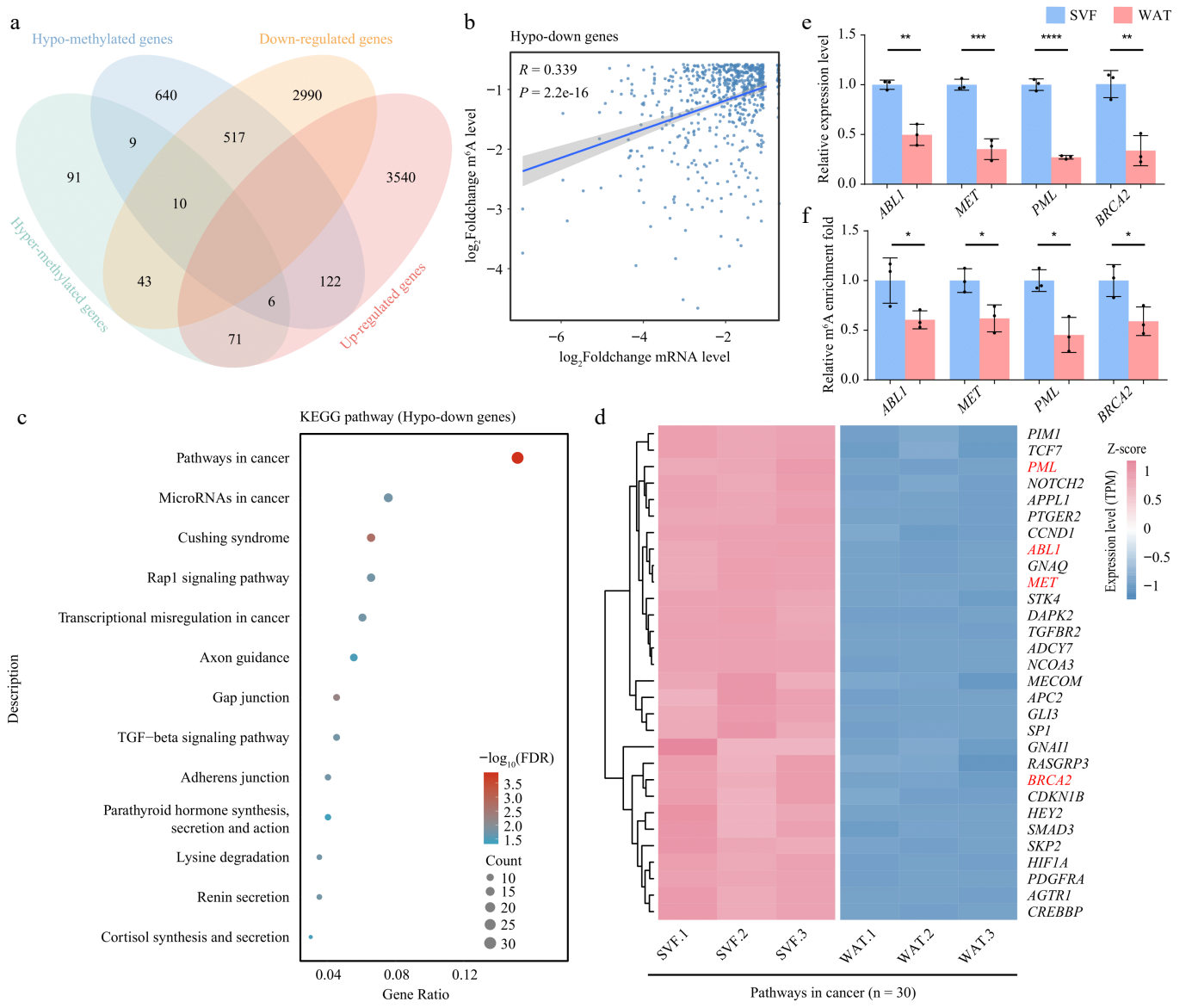

Fig. 5 m^{6}A demethylation correlates with transcriptome reprogramming during adipocyte differentiation. (a) Venn diagram showing the overlap between differentially methylated genes and differentially expressed genes. (b) Scatter plot illustrating the correlation between fold changes in m^{6}A modification levels and gene expression levels in hypo-down genes. Correlation was assessed using Pearson's method. (c) KEGG pathway enrichment analysis of hypo-down genes displayed as a bubble plot. (d) Heatmap of expression levels of cancer signaling pathway genes in SVF and WAT.(e) Expression levels, and (f) m^{6}A modification levels of selected hypo-down genes. β-actin was used as the internal reference gene. Error bars represent mean ± s.d. (n = 3). Statistical significance was determined using Student's t-test relative to day 0. $p < 0.05$; * $p < 0.01$; ** $p < 0.001$; *** $p < 0.0001$; ns, not significant ($p \geq 0.05$).

Further analysis identified several lipogenesis-related genes with altered methylation patterns. Genes such as forkhead box O3 (*FOXO3*), peroxisome proliferator-activated receptor delta (*PPARD*), fatty acid binding protein 4 (*FABP4*), retinol binding protein 5 (*RBP5*), and solute carrier family 7 member 2 (*SLC7A2*) were classified as hypo-up category. Two lipid metabolism genes, acetyl-CoA carboxylase alpha (*ACACA*), and peroxisome proliferator-activated receptor gamma (*PPARG*), which showed no change in m^{6}A modification in MeRIP-seq, were used as controls. Validation by MeRIP-qPCR and RT-qPCR confirmed that *FOXO3*, *FABP4*, *PPARD*, and *RBP5* showed reduced m^{6}A modification, consistent with MeRIP-seq data, whereas *SLC7A2* did not (Fig. 6a, b). Although some lipogenesis-related genes displayed hypo-methylation, most upregulated lipid metabolic genes did not exhibit significant changes in m^{6}A modification. Thus, while m^{6}A may contribute to the regulation of specific lipogenic genes, it is unlikely to be the dominant driver of their increased expression during adipocyte differentiation.

Together, these findings indicate that m^{6}A demethylation by erasers represses regulators of metabolism and transcription in WAT, selectively affects lipogenic genes, and links adipocyte differentiation to oncogenic pathways.

Discussion

Adipocyte differentiation and lipid metabolism are coordinated by complex transcriptional and post-transcriptional networks. The nuclear receptor peroxisome proliferator-activated receptor gamma (PPARγ), together with CCAAT/enhancer-binding protein alpha (C/EBPα) and other transcription factors, orchestrates the

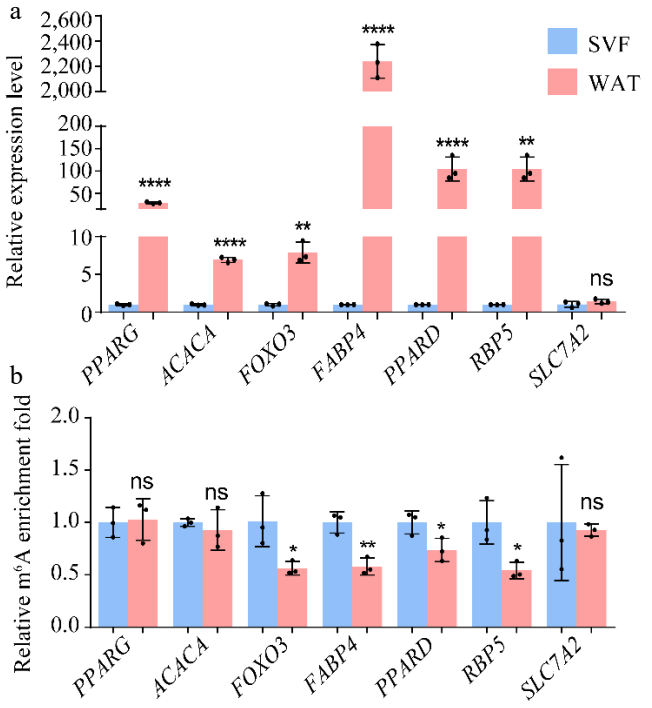

Fig. 6 (a) Expression levels and (b) m^{6}A modification levels of hypo-up genes. β-actin was used as the internal reference gene. Error bars represent mean ± s.d. (n = 3). Statistical significance was assessed using Student's t-test relative to day 0. * $p < 0.05$; ** $p < 0.01$; *** $p < 0.001$; **** $p < 0.0001$; ns, $p \geq 0.05$.

adipogenic transcriptional program required for terminal differentiation[45,51,52]. While numerous transcriptional regulators of adipogenesis have been identified[53], post-transcriptional regulation by m^{6}A has recently emerged as a key layer of control. In this study, we observed stage-specific dynamics of m^{6}A regulators: *Mettl14* expression increased during adipocyte differentiation, consistent with its essential role in maintaining adipocyte viability and metabolic homeostasis[54], whereas the demethylases *FTO* and *ALKBH5* remained highly expressed throughout differentiation, in line with their established functions in adipogenesis and lipid metabolism[55,56]. Transcriptome-wide analysis revealed that WAT is characterized by extensive m^{6}A hypo-methylation, correlating with reduced expression of genes involved in metabolic regulation and transcription. These findings highlight m^{6}A demethylation as a central mechanism shaping the transcriptome during porcine adipocyte differentiation, and provide mechanistic insight into adipose biology and metabolic regulation. Beyond adipogenesis, it was found that hypo-methylated and downregulated genes were significantly enriched in cancer-related pathways. Adipocytes are major stromal components that actively contribute to the tumor microenvironment by supplying energy substrates, regulating metabolism, and releasing adipokines. Cancer-associated adipocytes (CAAs) engage in reciprocal crosstalk with tumor cells, fueling growth and metastasis through free fatty acid release, fatty acid oxidation, and adipokine signaling[57–59]. The present results suggest that m^{6}A-dependent regulation of adipogenesis may influence the abundance and activity of adipocytes in the tumor microenvironment, thereby affecting cancer progression.

To further validate the positive correlation between m^{6}A demethylation and reduced expression of genes involved in the adipogenesis regulatory pathway and cancer-related pathway, the expression levels of these potential target genes should be quantified in FTO- or ALKBH5-knockdown cells. Moreover, assessing the adipogenic differentiation capacity of FTO- or ALKBH5-knockdown cells could further elucidate the critical regulatory role of m^{6}A demethylation in adipogenic differentiation. In addition, overexpressing m^{6}A methyltransferases (e.g., METTL14 or METTL16) in cells to restore the m^{6}A levels of hypomethylated lipid metabolism-associated genes-followed by evaluating the expression of adipogenesis/metabolism-related genes and the status of adipogenic differentiation under this condition, would provide additional evidence to support the notion that m^{6}A demethylation drives adipogenesis and metabolic reprogramming.

With the advancement of m^{6}A editing tools, precise m^{6}A RNA editing systems have been developed by fusing catalytically dead Cas (dCas) proteins with m^{6}A methyltransferases (e.g., METTL3 and METTL14) or m^{6}A demethylases (e.g., ALKBH5 and FTO)[60,61], enabling the functional characterization of individual genes. Guided by a single-guide RNA (sgRNA) targeting the gene of interest, the m^{6}A RNA editing system can precisely recognize the target gene and mediate site-specific m^{6}A methylation or demethylation, either in the nucleus or cytoplasm, depending on the type of fused catalytic protein. Furthermore, emerging integrated m^{6}A editing technologies, such as adenosine-to-inosine (A-to-I) editing and dCasRx-based editing, empower researchers to dissect the functional roles of individual m^{6}A modifications[62,63]. The present study identified a certain number of genes that exhibit significant m^{6}A modification changes during adipogenesis and may be involved in regulating porcine adipogenesis and cancer-related pathways. These genes could serve as ideal targets for m^{6}A RNA editing systems, providing a means to modulate porcine adipogenic differentiation or cancer cell differentiation. Targeted m^{6}A editing of key regulators may therefore represent a promising approach for precision livestock breeding and therapeutic strategies targeting lipid metabolism in cancer.

Conclusions

m^{6}A modification, a central mechanism of RNA epigenetic regulation in eukaryotes, plays a pivotal role in regulating physiological processes including growth, development, and metabolic homeostasis. Currently, research on m^{6}A modification has been widely applied in the analysis of pathological mechanisms and the exploration of potential intervention targets for major human diseases, including obesity, diabetes, neurological disorders, and malignant tumors. In contrast, studies on the functional roles of m^{6}A modification in livestock species remain limited. Using porcine adipocytes as a model, the present study systematically characterized the dynamic m^{6}A modification landscape and reveal key candidate targets within the m^{6}A-mediated regulatory network governing porcine fat deposition, filling the knowledge gap about m^{6}A role in porcine adipogenesis, and implicates m^{6}A in the functional interplay between adipose tissue and cancer, which could be used in developing m^{6}A-based precision editing tools for trait improvement in agricultural animals and supports the advancement of epigenetic breeding strategies in animal agriculture.

Ethical statements

All procedures were reviewed and approved in advance by the Institutional Animal Care and Use Committee of the Institute of Zoology, Chinese Academy of Sciences (Beijing, China) (Approval ID: IOZ-IACUC-2021-080, Approval date: 2021.08.03). The study adhered

to the principles of Replacement, Reduction, and Refinement to minimize animal suffering. Detailed information on animal housing, care, and pain management is provided to ensure that the welfare of the animals was maintained throughout the experiment.

Author contributions

The authors confirm their contributions to the paper as follows: study conception and design: Zhang X, Zhao J; methodology: Xie L, Huang J, Liu T, Liu Y; investigation: Huang J, Liu T, Liu Y; formal analysis: Xie L, Chen J; draft manuscript preparation: Xie L, Huang J, Liu T, Liu Y; writing – review and editing: Zhang X, Zhao J, Wang Q, Wang M, Chen J; funding acquisition: Zhang X, Huang J; supervision: Zhang X, Zhao J, Wang Q, Wang M, Chen J. All authors reviewed the results and approved the final version of the manuscript.

Data availability

All data generated or analyzed in this study are included in this published article and its supplementary information files. Raw datasets are available from the corresponding authors upon reasonable request.

Acknowledgments

This work was supported by Biological Breeding-National Science and Technology Major Project (2024ZD04077), the National Natural Science Foundation of China (NSFC U25A20678 and 32325042), Beijing Municipal Natural Science Foundation (6262020) and the Initiative Scientific Research Program, the Institute of Zoology, Chinese Academy of Sciences (2023IOZ0203 and 2024IOZ0106).

Conflict of interest

The authors declare that they have no conflict of interest.

Supplementary information accompanies this paper online at (https://doi.org/10.48130/epi-0025-0016)

Dates

Received 25 September 2025; Revised 10 November 2025; Accepted 2 December 2025; Published online 27 January 2026

References

[1] Wood JD, Enser M, Fisher AV, Nute GR, Sheard PR, et al. 2008. Fat deposition, fatty acid composition and meat quality: a review. *Meat Science* 78:343–358

[2] Zheng Q, Lin J, Huang J, Zhang H, Zhang R, et al. 2017. Reconstitution of UCP1 using CRISPR/Cas9 in the white adipose tissue of pigs decreases fat deposition and improves thermogenic capacity. *Proceedings of the National Academy of Sciences of the United States of America* 114:E9474–E9482

[3] Meurens F, Summerfield A, Nauwynck H, Saif L, Gerdts V. 2012. The pig: a model for human infectious diseases. *Trends in Microbiology* 20:50–57

[4] Fan N, Lai L. 2013. Genetically modified pig models for human diseases. *Journal of Genetics and Genomics* 40:67–73

[5] Rong P, Mu Y, Wang M, Chen L, Liu F, et al. 2025. Targeting IGF1 to alleviate obesity through regulating energy expenditure and fat deposition. *Science China Life Sciences* 68:1662–1675

[6] Keles U, Ow JR, Kuentzel KB, Zhao LN, Kaldis P. 2022. Liver-derived metabolites as signaling molecules in fatty liver disease. *Cellular and Molecular Life Sciences* 80:4

[7] Zhao BS, Roundtree IA, He C. 2017. Post-transcriptional gene regulation by mRNA modifications. *Nature Reviews Molecular Cell Biology* 18:31–42

[8] Boulias K, Greer EL. 2023. Biological roles of adenine methylation in RNA. *Nature Reviews Genetics* 24:143–160

[9] Dominissini D, Moshitch-Moshkovitz S, Schwartz S, Salmon-Divon M, Ungar L, et al. 2012. Topology of the human and mouse m^{6}A RNA methylomes revealed by m^{6}A-seq. *Nature* 485:201–206

[10] Linder B, Grozhik AV, Olarerin-George AO, Meydan C, Mason CE, et al. 2015. Single-nucleotide-resolution mapping of m^{6}A and m^{6}Am throughout the transcriptome. *Nature Methods* 12:767–772

[11] Liu J, Yue Y, Han D, Wang X, Fu Y, et al. 2014. A METTL3–METTL14 complex mediates mammalian nuclear RNA *N*^{6}-adenosine methylation. *Nature Chemical Biology* 10:93–95

[12] Liu J, Dou X, Chen C, Chen C, Liu C, et al. 2020. *N*^{6}-methyladenosine of chromosome-associated regulatory RNA regulates chromatin state and transcription. *Science* 367:580–586

[13] Jia G, Fu Y, Zhao X, Dai Q, Zheng G, et al. 2011. *N*^{6}-methyladenosine in nuclear RNA is a major substrate of the obesity-associated FTO. *Nature Chemical Biology* 7:885–887

[14] Zheng G, Dahl JA, Niu Y, Fedorcsak P, Huang CM, et al. 2013. ALKBH5 is a mammalian RNA demethylase that impacts RNA metabolism and mouse fertility. *Molecular Cell* 49:18–29

[15] Wang X, Zhao BS, Roundtree IA, Lu Z, Han D, et al. 2015. *N*^{6}-methyladenosine modulates messenger RNA translation efficiency. *Cell* 161:1388–1399

[16] Wang X, Lu Z, Gomez A, Hon GC, Yue Y, et al. 2014. *N*^{6}-methyladenosine-dependent regulation of messenger RNA stability. *Nature* 505:117–120

[17] Shi H, Wang X, Lu Z, Zhao BS, Ma H, et al. 2017. YTHDF3 facilitates translation and decay of *N*^{6}-methyladenosine-modified RNA. *Cell Research* 27:315–328

[18] Xu C, Wang X, Liu K, Roundtree IA, Tempel W, et al. 2014. Structural basis for selective binding of m^{6}A RNA by the YTHDC1 YTH domain. *Nature Chemical Biology* 10:927–929

[19] Hsu PJ, Zhu Y, Ma H, Guo Y, Shi X, et al. 2017. Ythdc2 is an *N*^{6}-methyladenosine binding protein that regulates mammalian spermatogenesis. *Cell Research* 27:1115–1127

[20] Huang H, Weng H, Sun W, Qin X, Shi H, et al. 2018. Recognition of RNA *N*^{6}-methyladenosine by IGF2BP proteins enhances mRNA stability and translation. *Nature Cell Biology* 20:285–295

[21] Xiao W, Adhikari S, Dahal U, Chen YS, Hao YJ, et al. 2016. Nuclear m^{6}A reader YTHDC1 regulates mRNA splicing. *Molecular Cell* 61:507–519

[22] Roundtree IA, Luo GZ, Zhang Z, Wang X, Zhou T, et al. 2017. YTHDC1 mediates nuclear export of *N*^{6}-methyladenosine methylated mRNAs. *eLife* 6:e31311

[23] Liu N, Dai Q, Zheng G, He C, Parisien M, et al. 2015. *N*^{6}-methyladenosine-dependent RNA structural switches regulate RNA–protein interactions. *Nature* 518:560–564

[24] Roost C, Lynch SR, Batista PJ, Qu K, Chang HY, et al. 2015. Structure and thermodynamics of N^6-methyladenosine in RNA: a spring-loaded base modification. *Journal of the American Chemical Society* 137:2107–2115

[25] Wang X, Wu R, Liu Y, Zhao Y, Bi Z, et al. 2020. m^{6}A mRNA methylation controls autophagy and adipogenesis by targeting *Atg5* and *Atg7*. *Autophagy* 16:1221–1235

[26] Li Y, Zhang Y, Zhang T, Ping X, Wang D, et al. 2023. Rna M^{6}a methylation regulates glycolysis of beige fat and contributes to systemic metabolic homeostasis. *Advanced Science* 10:e2300436

[27] Wu R, Guo G, Bi Z, Liu Y, Zhao Y, et al. 2019. m^{6}A methylation modulates adipogenesis through JAK2-STAT3-C/EBPβ signaling. *Biochimica et Biophysica Acta (BBA) - Gene Regulatory Mechanisms* 1862:796–806

[28] Wu R, Chen Y, Liu Y, Zhuang L, Chen W, et al. 2021. m^{6}A methylation promotes white-to-beige fat transition by facilitating Hif1a translation. *EMBO Reports* 22:e52348

[29] Chao M, Wang M, Han H, Liu Y, Sun X, et al. 2024. Profiling of m^{6}A methylation in porcine intramuscular adipocytes and unravelling PHKG1 represses porcine intramuscular lipid deposition in an m^{6}A-dependent manner. *International Journal of Biological Macromolecules* 272:132728

[30] Lin J, Cao C, Tao C, Ye R, Dong M, et al. 2017. Cold adaptation in pigs depends on UCP3 in beige adipocytes. *Journal of Molecular Cell Biology* 9:364–375
[31] Chen S, Zhou Y, Chen Y, Gu J. 2018. fastp: an ultra-fast all-in-one FASTQ preprocessor. *Bioinformatics* 34:i884–i890
[32] Ewels P, Magnusson M, Lundin S, Käller M. 2016. MultiQC: summarize analysis results for multiple tools and samples in a single report. *Bioinformatics* 32:3047–3048
[33] Warr A, Affara N, Aken B, Beiki H, Bickhart DM, et al. 2020. An improved pig reference genome sequence to enable pig genetics and genomics research. *GigaScience* 9:giaa051
[34] Kim D, Paggi JM, Park C, Bennett C, Salzberg SL. 2019. Graph-based genome alignment and genotyping with HISAT2 and HISAT-genotype. *Nature Biotechnology* 37:907–915
[35] Liao Y, Smyth GK, Shi W. 2013. The Subread aligner: fast, accurate and scalable read mapping by seed-and-vote. *Nucleic Acids Research* 41:e108
[36] Love MI, Huber W, Anders S. 2014. Moderated estimation of fold change and dispersion for RNA-seq data with DESeq2. *Genome Biology* 15:550
[37] Ramírez F, Dündar F, Diehl S, Grüning BA, Manke T. 2014. deepTools: a flexible platform for exploring deep-sequencing data. *Nucleic Acids Research* 42:W187–W191
[38] Yu G, Wang LG, Han Y, He QY. 2012. clusterProfiler: an R package for comparing biological themes among gene clusters. *Omics* 16:284–287
[39] Yu G, Wang LG, He QY. 2015. ChIPseeker: an R/Bioconductor package for ChIP peak annotation, comparison and visualization. *Bioinformatics* 31:2382–2383
[40] Liu L, Zhang SW, Huang Y, Meng J. 2017. QNB: differential RNA methylation analysis for count-based small-sample sequencing data with a quad-negative binomial model. *BMC Bioinformatics* 18:387
[41] Heinz S, Benner C, Spann N, Bertolino E, Lin YC, et al. 2010. Simple combinations of lineage-determining transcription factors prime cis-regulatory elements required for macrophage and B cell identities. *Molecular Cell* 38:576–589
[42] Quinlan AR, Hall IM. 2010. BEDTools: a flexible suite of utilities for comparing genomic features. *Bioinformatics* 26:841–842
[43] Kanehisa M, Furumichi M, Sato Y, Ishiguro-Watanabe M, Tanabe M. 2021. KEGG: integrating viruses and cellular organisms. *Nucleic Acids Research* 49:D545–D551
[44] Fischer J, Koch L, Emmerling C, Vierkotten J, Peters T, et al. 2009. Inactivation of the *Fto* gene protects from obesity. *Nature* 458:894–898
[45] Tontonoz P, Spiegelman BM. 2008. Fat and beyond: the diverse biology of PPARgamma. *Annual Review of Biochemistry* 77:289–312
[46] Meyer KD, Saletore Y, Zumbo P, Elemento O, Mason CE, et al. 2012. Comprehensive analysis of mRNA methylation reveals enrichment in 3' UTRs and near stop codons. *Cell* 149:1635–1646
[47] Mao Y, Dong L, Liu XM, Guo J, Ma H, et al. 2019. m^{6}A in mRNA coding regions promotes translation via the RNA helicase-containing YTHDC2. *Nature Communications* 10:5332
[48] Zhang H, Shi X, Huang T, Zhao X, Chen W, et al. 2020. Dynamic landscape and evolution of m^{6}A methylation in human. *Nucleic Acids Research* 48:6251–6264
[49] Mandl M, Wagner SA, Hatzmann FM, Mitterberger-Vogt MC, Zwierzina ME, et al. 2019. Sprouty1 is a weight-loss target gene in human adipose stem/progenitor cells that is mandatory for the initiation of adipogenesis. *Cell Death & Disease* 10:411
[50] Ding F, Zheng P, Yan XY, Chen HJ, Fang HT, et al. 2024. Adipocyte-secreted PRELP promotes adipocyte differentiation and adipose tissue fibrosis by binding with p75(NTR) to activate FAK/MAPK signaling. *International Journal of Biological Macromolecules* 279:135376
[51] Lefterova MI, Haakonsson AK, Lazar MA, Mandrup S. 2014. PPARγ and the global map of adipogenesis and beyond. *Trends in Endocrinology & Metabolism* 25:293–302
[52] Guo L, Li X, Tang QQ. 2015. Transcriptional regulation of adipocyte differentiation: a central role for CCAAT/enhancer-binding protein (C/EBP) β. *Journal of Biological Chemistry* 290:755–761
[53] Lowe CE, O'Rahilly S, Rochford JJ. 2011. Adipogenesis at a glance. *Journal of Cell Science* 124:2681–2686
[54] Kang Q, Zhu X, Ren D, Ky A, MacDougald OA, et al. 2023. Adipose METTL14-elicited N^6-methyladenosine promotes obesity, insulin resistance, and NAFLD through suppressing β adrenergic signaling and lipolysis. *Advanced Science* 10:e2301645
[55] Merkestein M, Laber S, McMurray F, Andrew D, Sachse G, et al. 2015. FTO influences adipogenesis by regulating mitotic clonal expansion. *Nature Communications* 6:6792
[56] Chao X, Guo L, Ye C, Liu A, Wang X, et al. 2024. ALKBH5 regulates chicken adipogenesis by mediating LCAT mRNA stability depending on m^{6}A modification. *BMC Genomics* 25:634
[57] Wu Q, Li B, Li Z, Li J, Sun S, et al. 2019. Cancer-associated adipocytes: key players in breast cancer progression. *Journal of Hematology & Oncology* 12:95
[58] Attané C, Muller C. 2020. Drilling for oil: tumor-surrounding adipocytes fueling cancer. *Trends in Cancer* 6:593–604
[59] Cha YJ, Kim ES, Koo JS. 2018. Tumor-associated macrophages and crown-like structures in adipose tissue in breast cancer. *Breast Cancer Research and Treatment* 170:15–25
[60] Liu XM, Zhou J, Mao Y, Ji Q, Qian SB. 2019. Programmable RNA N^6-methyladenosine editing by CRISPR-Cas9 conjugates. *Nature Chemical Biology* 15:865–871
[61] Wilson C, Chen PJ, Miao Z, Liu DR. 2020. Programmable m^{6}A modification of cellular RNAs with a Cas13-directed methyltransferase. *Nature Biotechnology* 38:1431–1440
[62] Xiang JF, Yang Q, Liu CX, Wu M, Chen LL, et al. 2018. N^6-methyladenosines modulate A-to-I RNA editing. *Molecular Cell* 69:126–135.E6
[63] Xia Z, Tang M, Ma J, Zhang H, Gimple RC, et al. 2021. Epitranscriptomic editing of the RNA N^6-methyladenosine modification by dCasRx conjugated methyltransferase and demethylase. *Nucleic Acids Research* 49:7361–7374